Tomostatics:
Turning-ray tomography + static corrections

By XIANHUAI ZHU, DAVID P. SIXTA, and BURKE G. ANGSTMAN
Union Pacific Resources
Fort Worth, Texas

Applications of tomographic velocities to static corrections have drawn much attention recently. In *Computing field statics with the help of seismic tomography* (*Geophysical Prospecting* 1987), W.N. de Amorin et al. showed that the waves refracted at the base of a low-velocity layer can be used successfully for computing and refining field static corrections. In *Tomographic inversion for velocity plus statics* (*SEG Expanded Abstracts* 1991), Livia Squires et al. pointed out that velocity variations and static shifts caused by near-surface effects and positional uncertainties can be solved simultaneously using constraint tomography.

Examples presented in this paper illustrate that turning ray tomography can image near-surface velocities more accurately than refraction statics methods. Consequently, the shallow-velocity image estimated from tomography provides for more accurate short and long wavelength statics. This is of significant benefit because it provides for an optimal NMO velocity analysis and CMP stack response, a better migration image, and a more reliable depth conversion. The drawback to traveltime tomography is that it is still dependent on the quality of picked first arrivals.

In this article, turning ray (wave) concepts are briefly reviewed and illustrated with a synthetic example; the steps of tomographic imaging and static correction are summarized; and, in conclusion, one synthetic and two field data sets are presented.

Turning rays. First arrivals are commonly modeled using refraction (or head wave) ray theory. In this case, the near-surface model is typically comprised of several velocity layers. First arrivals represent refracted energy traveling along the interface between two layers. This model supports lateral changes in layer velocity but assumes there are no vertical velocity changes within each layer. However, field data observations suggest the presence of a vertical velocity gradient in the near surface due to the compaction of rocks. One such observation is the nonlinear behavior of first arrivals, indicating a gradually increasing apparent velocity with offset.

To accommodate a vertical velocity gradient, a turning-ray (or continuous refraction) model is proposed. In this case, first arrivals represent a wavefront traveling through a continuous velocity medium with vertical as well as horizontal velocity gradients. The presence of a gradient causes downgoing rays to turn (or continuously refract), eventually bending the rays upward to return to the surface. Some negative gradients (velocity inversions) are also supported in this model, provided the overall velocity field allows sufficient ray bending to return rays to the surface within the recording aperture. The use of turning rays in the imaging of salt dome flanks has been recently demonstrated in *Imaging salt with turning seismic waves* by Dave Hale et al. (*SEG Expanded Abstracts* 1991); *Application of turning wave migration to a 3-D seismic survey in Main Pass Block 299, Offshore Louisiana and its impact on field development* by William Foley et al. (*SEG Expanded Abstracts* 1991); *Salt-flank imaging using Gaussian beam migration* by N.R. Hill et al. (*SEG Expanded Abstracts* 1991); and *Seismic imaging of salt structures in the Gulf of Mexico* by Davis Ratcliff et al. (April 1992 *TLE*).

To illustrate the concept of turning rays (waves), a synthetic shot record was generated from a simple velocity model. The input model (Figure 1a) consists of two layers. Each layer velocity is continuous and increases with depth (positive gradient):

$$V1(z) = 1.10 + k1\ z \text{ km/s (for } 0<z<182 \text{ m), and}$$

$$V2(z) = 2.24 + k2\ z \text{ km/s (for } 188<z<800 \text{ m)}$$

where k1 = 4.67 and k2 = 2.68.

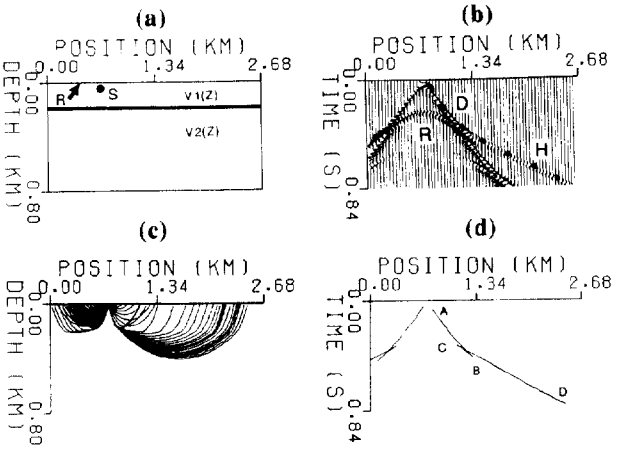

Figure 1. Comparison of first-arrivals using ray and wave simulations. (a) Velocity model contains two, V1(z) and V2(z), layers. Between the layers is a 6 m transition zone. Source is located at S, and recording line R is placed at the surface. (b) Seismograms simulated by acoustic finite-difference modeling; D is direct wave, R the reflected wave, H the apparent head wave. (c) Turning rays simulated by ray tracing. (d) The corresponding first arrivals superimposed on (b).

The two layers are separated by a thin, flat "transition zone" with a high-velocity gradient (velocities increase from 1.95 to 2.74 km/s over 6 m). This high-gradient zone is representative of an interface between the two layers.

An acoustic finite-difference algorithm was used to generate the synthetic shot record (Figure 1b) from the velocity model. The model size is 800 × 239 with a grid increment of 3.4 m. The time sampling interval is 0.5 ms and the dominant frequency is 5 Hz. The source time function is a Gaussian wavelet.

In Figure 1b, the reflected wave (R), the direct wave (D), and the apparent head wave (H) are clearly evident and labeled. Although difficult to see, both D and H behave nonlinearly (slopes increasing with offset). These nonlinear effects in D and H are caused by the velocity gradients in the first and second layers, respectively. If the gradient in the second layer was absent, the apparent head wave would behave linearly.

To further illustrate this concept, ray tracing was also performed on the velocity model. Raypaths from the modeling are displayed in Figure 1c. Note how the apparent head-wave raypaths dive into the second layer before turning upward. In Figure 1d, the ray traveltimes are displayed. A caustic (triplication), due to the sudden velocity increase within the transition zone, is evident. In Figure 1d, as discussed by K. Aki and P. Richards in *Quantitative Seismology* (Freeman Press, 1980), branch AB may be called the direct ray, branch BC is a reflection-like ray, and branch CD is a head-wave-like ray. The first arrivals from the ray tracing are superimposed on top of the first arrivals from acoustic modeling. There is excellent agreement between the wave theory and ray theory traveltimes.

This test model helps demonstrate the significance of turning rays (waves). The presence of turning waves in the first arrivals is necessarily implied by a distinctive nonlinear behavior. Most field records appear to manifest this behavior. Consequently, the turning-ray model appears appropriate for modeling first arrivals.

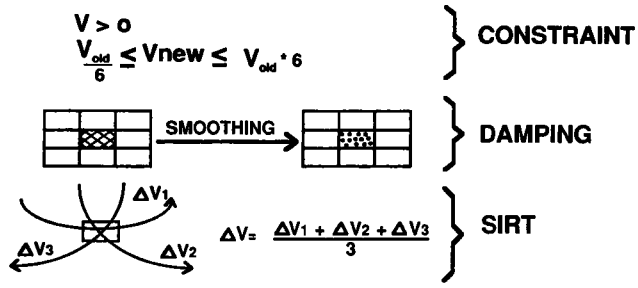

Figure 2. The Constrained Damped Simultaneous Iterative Reconstruction Technique (CDSIRT).

Tomographic imaging. The medium to be imaged is discretized into a grid of small rectangular elements or cells, each of which contains a single velocity V. The input data are traveltimes (t) from first arrivals. Sources and receivers are both located on the surface. Velocity estimation is performed by the solution of the system of equations

$$\mathbf{t} = \underset{\sim}{\mathbf{D}}\,\mathbf{s}$$

where $\mathbf{t}$ is the $m \times 1$ column vector of time observations, $\underset{\sim}{\mathbf{D}}$ is the $m \times n$ matrix of ray segments, and $\mathbf{s}$ is the $n \times 1$ vector of unknown slownesses (slowness being the reciprocal of velocity). The solution involves minimization of the differences between the observed (picked) and predicted (ray traced from an initial model) traveltimes. It is equally applicable to under- and overdetermined problems.

The solution is iterative, containing five steps:

1) Picking of first arrivals
2) Ray tracing through an initial estimate of the velocity model
3) Segmenting of raypaths into the portion contained in each cell of the velocity model
4) Computing the differences between the observed and

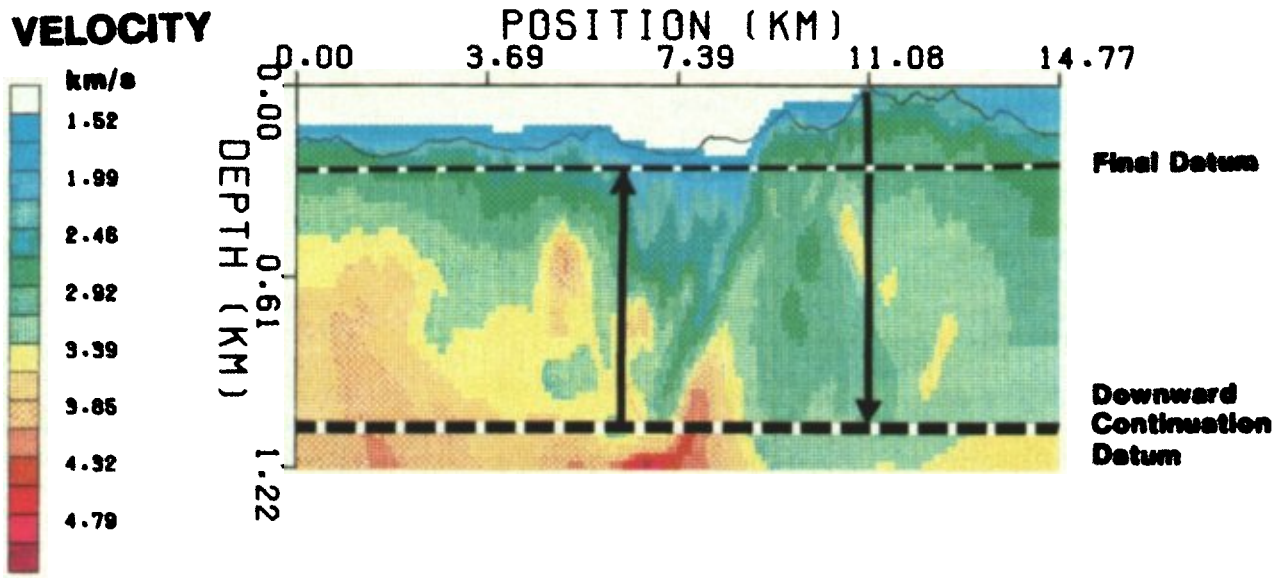

Figure 3. The calculated static time shifts based upon a tomographic image of an overthrust seismic profile (see Figures 9a and 9b). Color scale indicates velocities in km/s.

predicted times for each ray

5) Iteratively back projecting the time differences to produce velocity model updates

During the back projection, the amount of velocity adjustment in each cell can be constrained using a trade-off between stability and convergence (Figure 2). Once all rays have been examined, the velocity field is updated using an average correction for each cell. The average corrections can be further constrained by knowledge of rock velocities in the area. The updated velocities are slightly smoothed (or damped) every few iterations. This is the Constrained Damped Simultaneous Iterative Reconstruction Technique (CDSIRT). J. Trampert and J.J. Levesque have shown in *Simultaneous iterative reconstruction technique: Physical interpretation based on the generalized least squares solution* (*Journal of Geophysical Research* 1990) that DSIRT is equivalent to generalized least squares inversion (GLI). It is important to have rays densely and evenly distributed at independent angles through each velocity cell.

Static corrections. The procedure to calculate tomostatics in this paper is very straightforward. Shot and receiver static corrections (Figure 3) are calculated vertically from the surface to a downward continuation datum using the computed near-surface velocity field. Upward continuation to a final datum, using a constant replacement velocity, is additionally performed via a bulk static shift.

Statics derived from near-surface models are usually helpful for removing long wavelength (> ½ cable length) statics. On the other hand, residual statics are useful for correcting short wavelength (< ½ cable length) statics. In practice, both refraction statics and tomostatics are good for calculating short and long wavelength static corrections. Nevertheless, some short wavelength statics may remain. Therefore, residual statics are desirable and were applied to all field data examples presented in this paper.

After the application of tomostatics, NMO velocities should be reanalyzed due to the coupling of statics and velocities. This is an important step in optimizing the stack image.

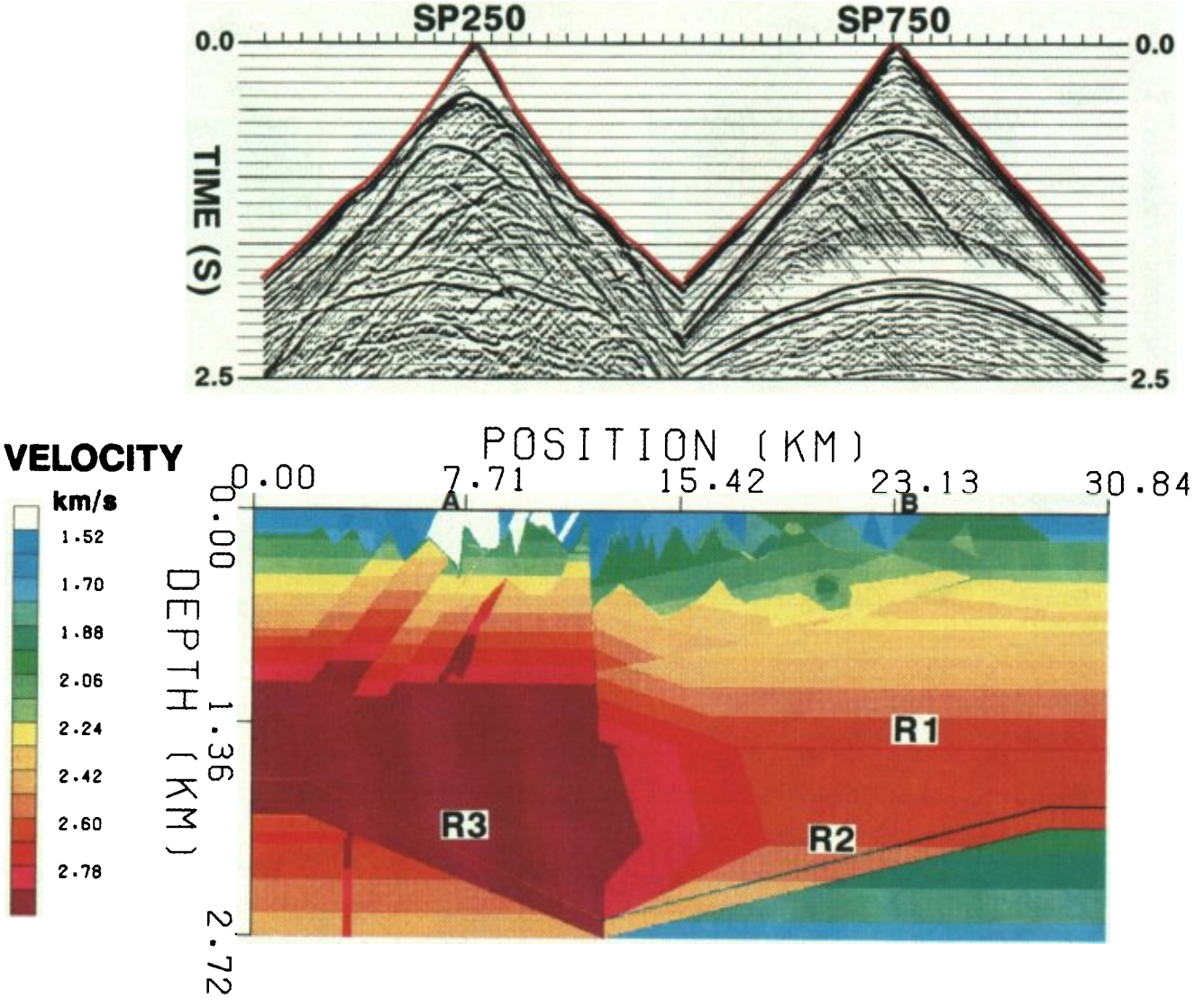

Figure 4. A velocity model containing complicated near-surface velocity variations. Color scale indicates velocities in km/s. Two representative synthetic common shot gathers recorded at locations A and B are shown on the top which were generated by acoustic finite-difference modeling. First arrivals picked are indicated with red lines.

Synthetic example. In order to demonstrate the utility of tomostatics to solve short and long wavelength static problems, a comparison of tomostatics with elevation and refraction statics was carried out using a synthetic data set. These data were provided by Advance Geophysical Corporation using a finite-difference algorithm. The data set consisted of 352 shot records, each containing 220 channels. The group interval was 34 m and the maximum offset was 3600 m. Figure 4 shows the model (bottom) and two representative shot records (top), recorded at locations A and B. The model has a flat surface topography with complicated velocity variations near the surface. Major reflection events evident on the shot records were generated from interfaces (R1, R2, and R3) deeper in the model. Due to the near-surface velocity variations, both reflections and diffractions on the shot records are distorted and no longer hyperbolic.

The initial model (Figure 5, upper left) was estimated from the shot records by "pencil and ruler" measurements of apparent velocities. The rectangular grid elements used in the tomography step had dimensions of the group interval (34 m)

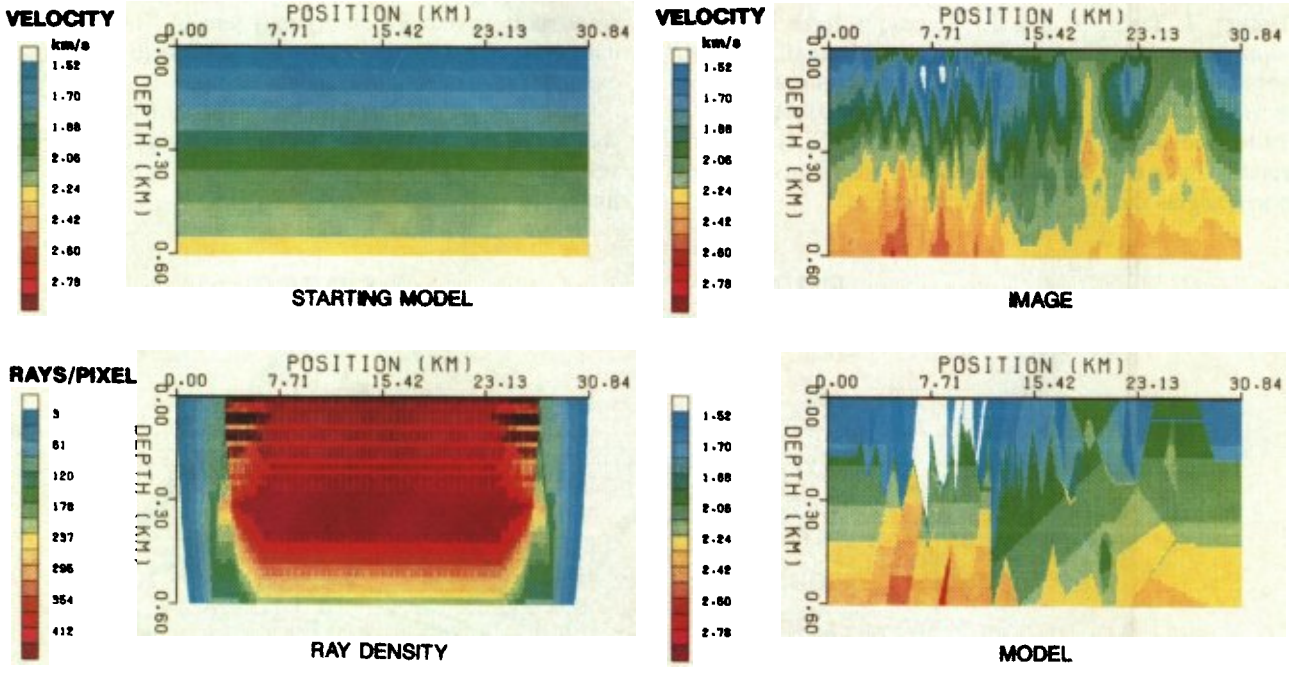

Figure 5. Tomographic velocity distributions after 0 (upper left) and 36 (upper right) iterations of the synthetic model (Figure 4). The ray density (lower left) was traced in the starting model (upper left) to generate image (upper right). True model is shown in the lower right.

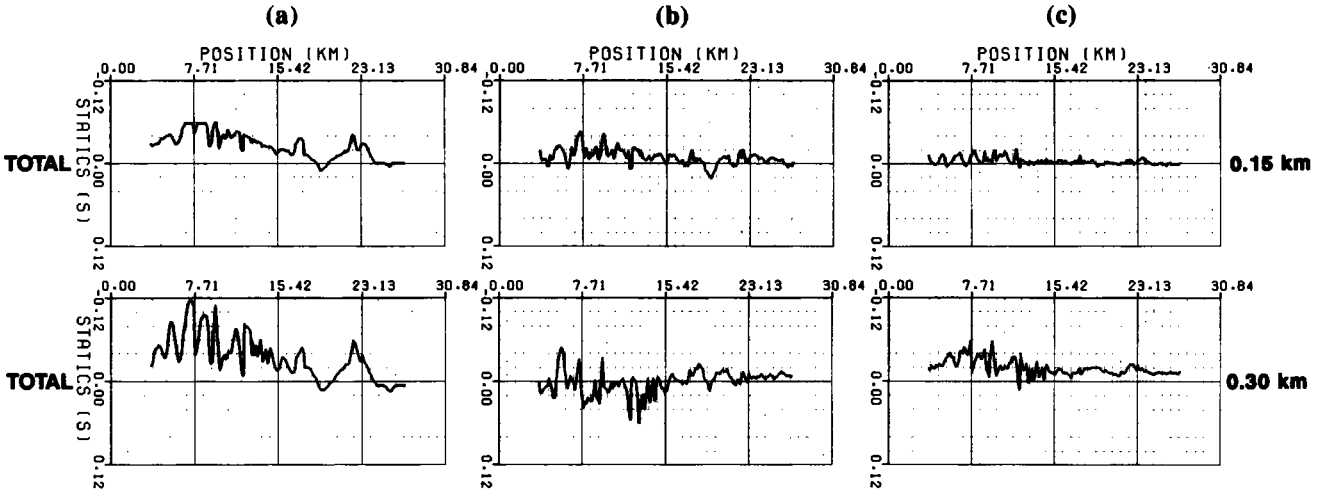

Figure 6. Total statics calculated vertically from the surface to a depth of 150 m (upper panels) and 300 m (lower panels). (a) True statics from the model; (b) difference between the true statics and refraction statics; and (c) difference between the true statics and tomostatics.

horizontally and half this amount (17 m) vertically. This principle was applied to all examples presented in this paper. A total of 176 shot records (every other generated shot) was used to obtain the velocity image. Figure 5 (upper right) is the velocity image after 36 iterations. (The true velocity model, the lower right of Figure 5, was not released by Advance until the tomographic velocity image was obtained.) The image is reliable only within the region sampled by the rays (Figure 5, lower left). The average time residual decreased from 109 ms/ray from the starting model to 2.6 ms/ray at iteration 36, which indicates convergence. It is important to note that there is no obvious correlation between the ray density and the velocity image. This indicates that the given ray density is sufficient to resolve the actual velocity variations that are present.

Figure 6 shows the total (shot + receiver) statics calculated for downward continuation datums of 150 m (top panels) and 300 m (bottom panels). The two panels marked (a) in Figure 6 are the true statics computed from the model. Those marked (b) are the differences between the true statics and refraction statics, and the ones marked (c) are the differences between the true statics and tomostatics. In Figures 6b, refraction statics estimated at 150 m were based on a one-layer model using offsets between 200 and 2300 m. At 300 m, the refractions statics were based upon a two-layer model using all offsets. The refraction solutions were calculated using the hybrid Extended Generalized Reciprocal Method (EGRM) and the Gauss-Seidel (least squares) iteration technique.

Analysis of Figure 6 shows that computed tomostatics are closer to those for the true model than those for refraction statics. Tomostatics are noticeably closer to the true statics where velocity inversions are significant (spatial positions near 19 km). Long spatial wavelength statics appear to be estimated better using tomostatics, although a tomostatics bias (bulk shift) exists with increasing depth. This is due to the use of a single ray tracing through the initial model (linear tomographic inversion). The accuracy of deep velocities can be increased by the use of nonlinear tomographic inversion (multiple ray tracings with iterative model updates).

The differences between refraction statics and tomostatics were further illustrated by stacking the data. Figure 7 shows the stacked time sections with elevation statics (upper left), refraction statics (upper right), tomostatics (lower left), and true statics (lower right). All static corrections were computed to a downward continuation datum of 300 m. A constant replacement velocity of 1.98 km/s was used for subsequent upward continuation to the surface. In order to separate the effect of statics from NMO velocities, the same NMO velocity profile was applied to all the stacks.

It is clear that the section with tomostatics has done a better job of resolving both the short and long wavelength statics than the section with refraction statics. Also, the time dips (R1, R2, and R3) and the diffraction patterns (D) after tomostatics more closely resemble those achieved by the true statics. This indicates that the stacked time section using tomostatics will tend to have a better image after migration.

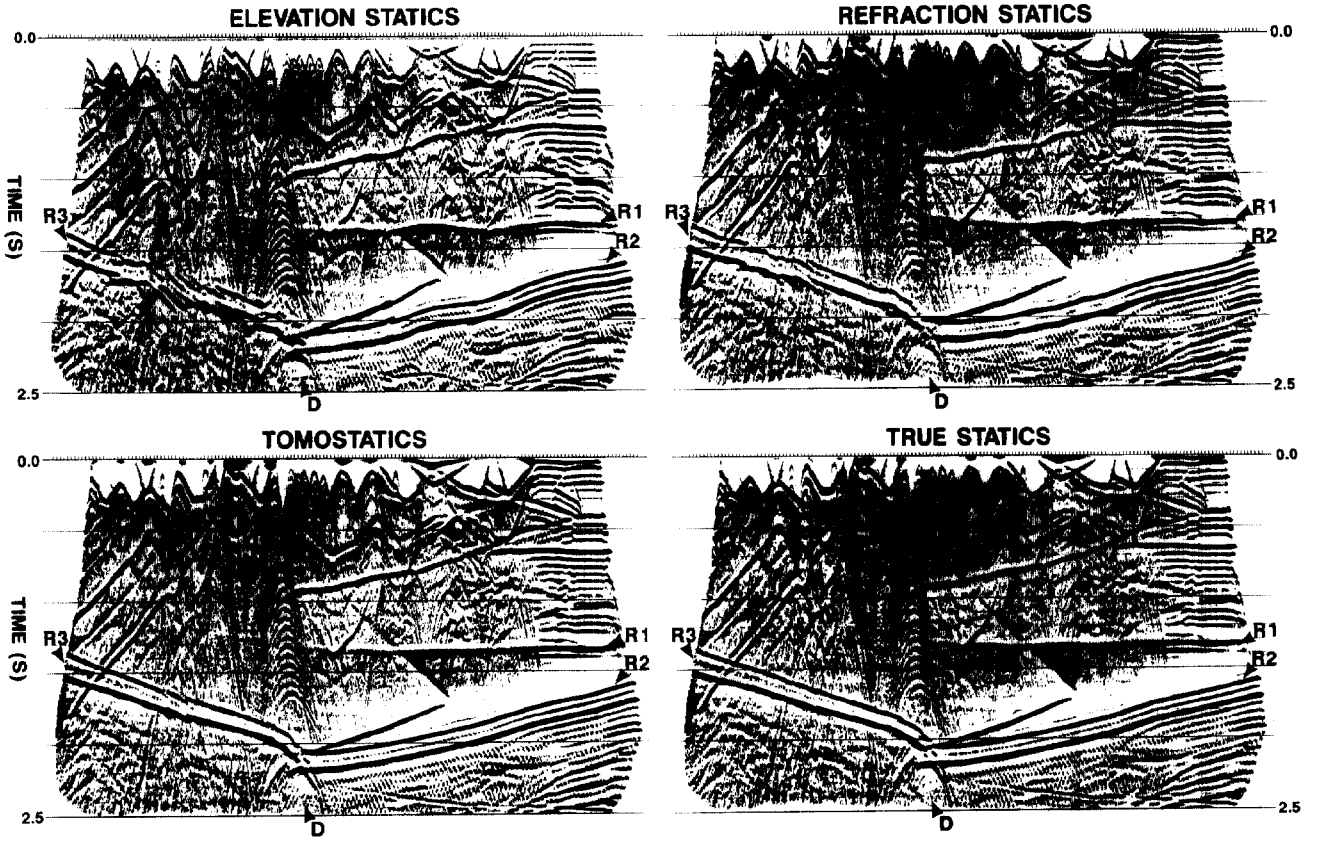

Figure 7. Stacked sections with elevation statics (upper left), refraction statics (upper right), tomostatics (lower left), and true statics (lower right). Reflection events from interfaces R1, R2, and R3 are labelled with symbols. D are diffractions generated along the fault (see Figure 4).

Field data examples. The improvement on short and long wavelength statics using tomostatics is further illustrated by examples from the Austin chalk and overthrust areas.

Horizontal drilling is an effective technique for exploration in the Austin chalk trend. The target zone is usually only 6-30 m thick. As a result, accurate time structure maps are required to predict subsurface dip ahead of drilling. A 5 ms difference in the time structure may have a significant impact on the horizontal drilling success.

Figure 8a shows the migrated time section of a vibroseis line recorded from the Austin chalk area in 1991. The recording geometry is split-spread, with a group interval of 25 m. The maximum offset is equal to the fixed cable length of 2300 m. The recording fold reached a maximum of 60 at the center of the line and tapered down to 1 at either end. In Figure 8a, only elevation statics and residual statics were applied. The bow-like time structure suggested a poor long wavelength solution and the results were considered invalid. Consequently, they were not used to predict geologic dip ahead of drilling. Using only well control to estimate the regional dip caused the horizontal well to miss the target zone.

Subsequent to this drilling effort, additional work was

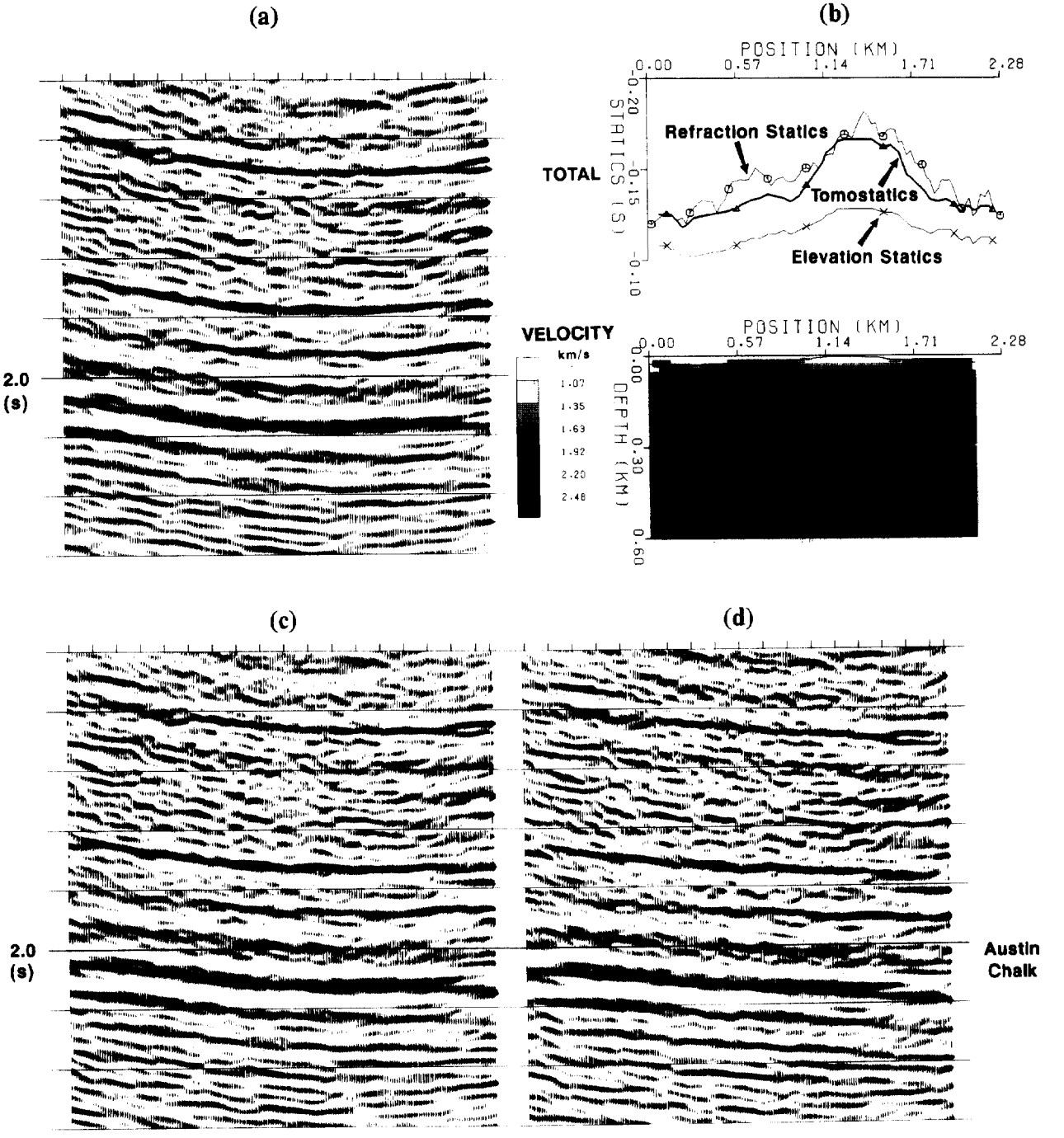

Figure 8. Migrated time sections of a vibroseis line recorded from the Austin chalk area: (a) elevation statics; (c) refraction statics; (d) tomostatics. Residual statics were applied to (a), (c), and (d). (b) Tomographic image. Total (shot + receiver) statics are plotted at the top.

performed to better estimate the long wavelength statics solution. It became clear that this was an important processing step if the seismic data were to have any economic benefit. Figure 8c shows the migrated time section after refraction statics. The refraction solution was calculated to a depth of 55 m from the surface and shifted back to the final datum using a replacement velocity of 1.8 km/s.

Figure 8d shows the migrated time section after tomostatics. The tomostatics were computed from the surface to a downward continuation datum of 300 m (dashed line in Figure 8b) and upward continued to the final datum using a replacement velocity of 2.0 km/s. The velocity image was obtained after 18 iterations (using only one ray trace) and was based on a 1-D initial velocity model. The peaks of the long wavelength statics correspond to a low-velocity zone at the shallow part of the image. It is obvious that the chalk events on the migrated section with tomostatics are much flatter than those with either elevation statics or refraction statics. Also, fault locations are more clearly visible. A key point is that tomostatics provided a more accurate time structure, resulting in a better migrated image. The converted depth section using the tomostatics stack is consistent with the depth structure measured independently from a formation microscanning (FMS) tool.

A successful application to a line from an overthrust area demonstrates that tomostatics are also feasible for complicated structures. For this data set, the recording geometry is split-spread, with a group interval of 50 m and a maximum offset of 6000 m. Figure 9a shows the unmigrated stacked section across the overthrust line using refraction statics. A one-layer model was used and the maximum depth computed was 90 m. The improved stacked section with tomostatics is

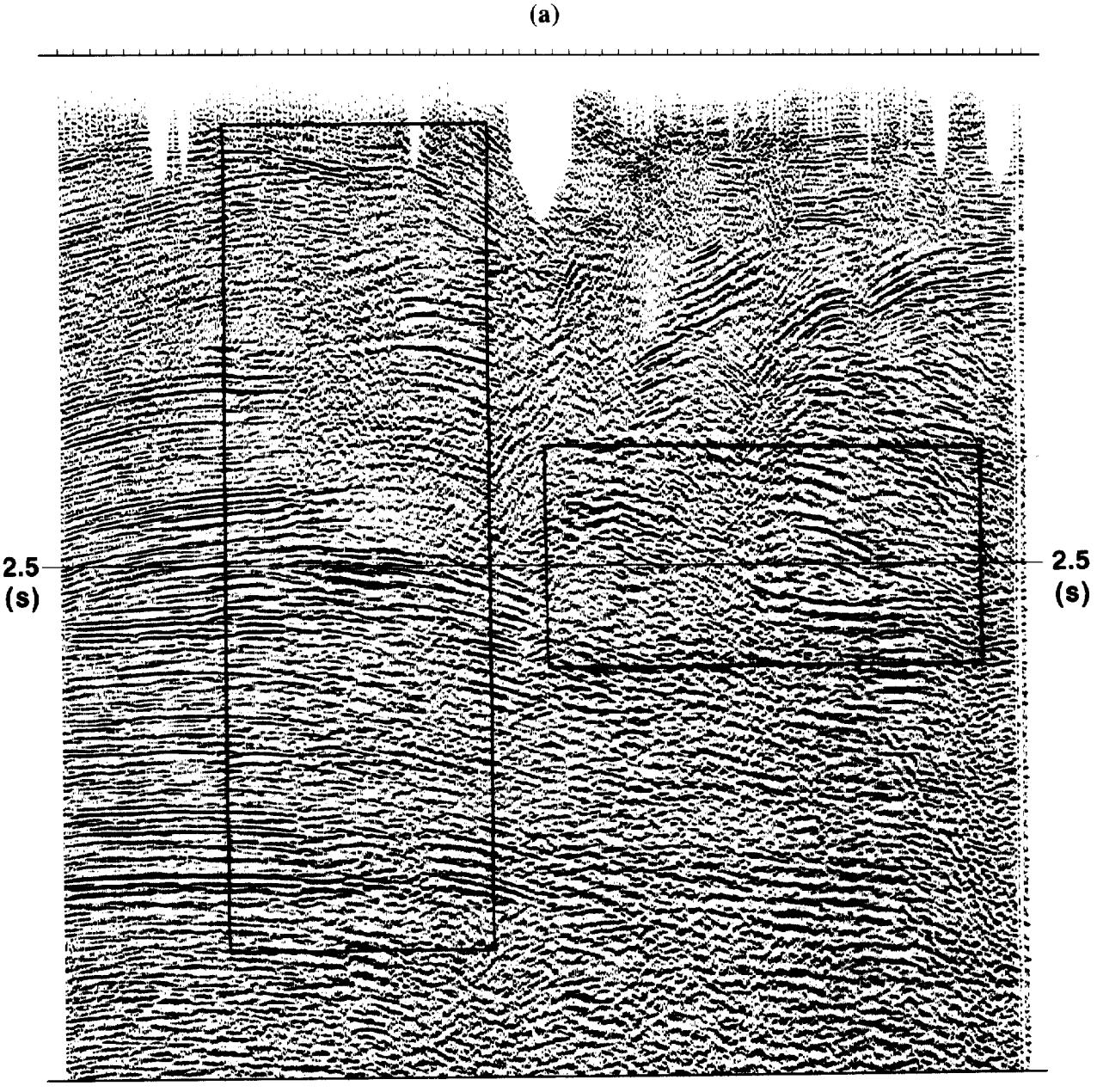

Figure 9a. Stacked section of a line from an overthrust area with refraction statics and residual statics.

shown in Figure 9b. Note the enhanced resolution in both the vertical and horizontal directions. The tomographic velocity image is shown in Figure 3. It was obtained after 18 iterations (using only one ray trace) starting from a 2-D initial model estimated using well log data. The downward continuation datum is 1000 m below the highest surface elevation. The improved time structures obtained using tomostatics are consistent with previous geologic interpretations and well log information.

Conclusions. First-arrival tomography—incorporating turning-ray (or continuous refraction) forward modeling—is a viable technique for imaging the near-surface velocity profile. As with refraction statics, the output velocity field may be utilized to compute downward-continuation statics. Turning-ray tomography differs from conventional refraction statics in the following ways:

- *Turning-ray model versus refracting-interface model.* In tomography, observed first-arrival traveltimes are inverted via turning-ray forward modeling through an initial discretized velocity field and iterative velocity field updates estimated from observed-versus-modeled traveltime differences. The use of turning rays is significant. It has been observed that first arrivals are often best simulated using a turning-ray model rather than a layered, refracting-interface model.

- *Gridded-output velocities versus layered-output velocities.* Unlike refraction statics, tomography does not require the near-surface velocity profile to be output in terms of

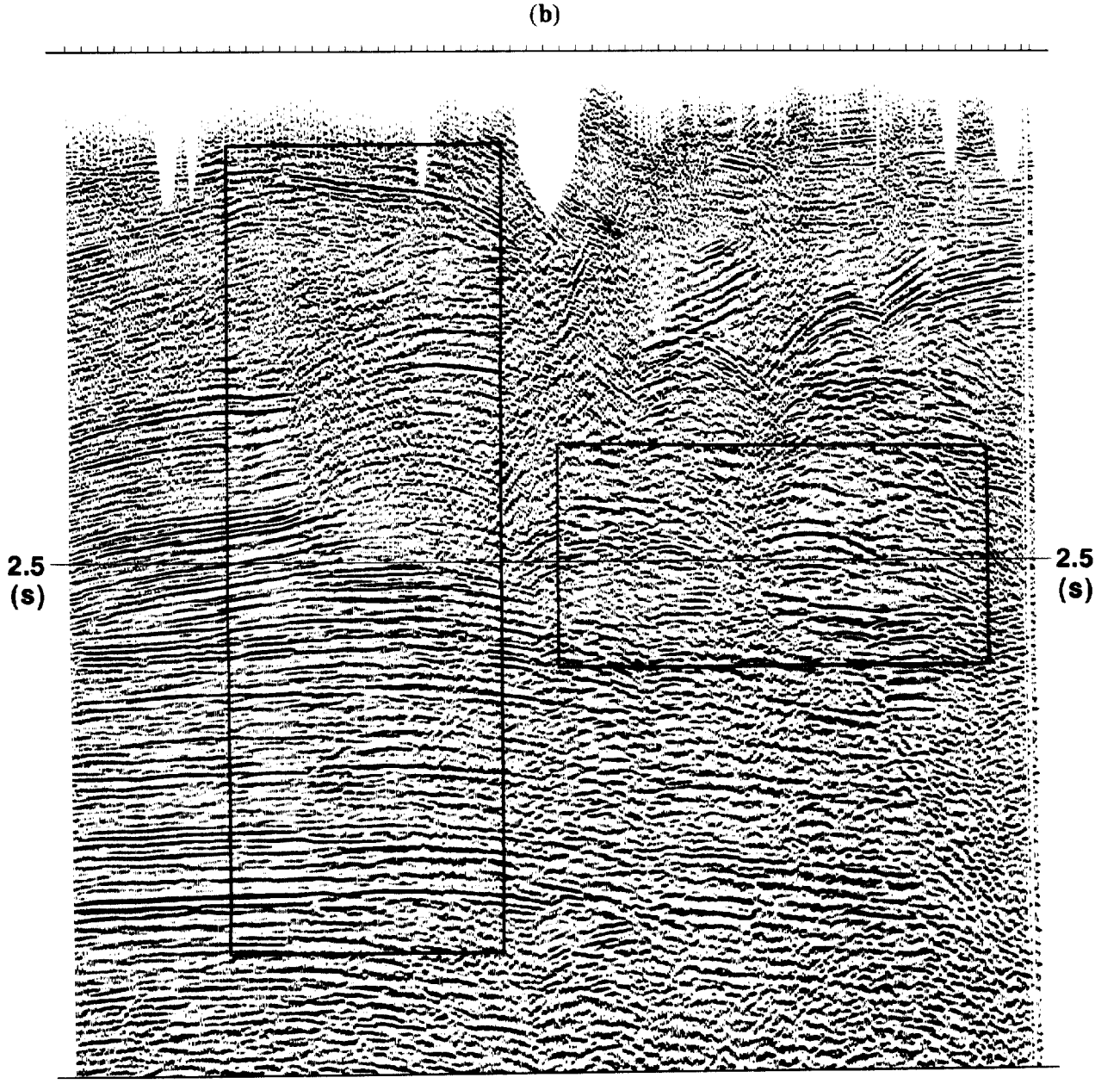

Figure 9b. Stacked section of the overthrust line in Figure 9a with tomostatics and residual statics.

layers. First-arrival tomography outputs the velocity field as a rectangular grid of constant velocity cells. Velocity cells with a width of a group interval allow for a remarkably good structural image of the near surface. This is particularly useful for complex geologic settings.

• *Velocity may decrease with depth versus velocity must increase with depth.* Some velocity decrease with depth is possible with turning-ray modeling. This is true when the overall velocity gradient allows sufficient ray bending to return rays to the surface within the recording aperture. In refraction statics, the refracting-interface model does not allow for a velocity which decreases with depth.

• *"V-zero" velocity computed versus required input of "V-zero."* For the proposed linearized (one ray tracing) tomographic inversion, computed velocities are more accurate immediately beneath the surface topography and decrease in accuracy with depth. In contrast, the shallowest velocities (so called "V-zero") from refraction solutions are frequently inaccurate, being estimated from either near-offset direct arrivals or regional information. Since velocities are usually most variable at shallow depths, tomography can potentially yield output models more accurate than those from refraction methods. For most velocity gradients, a distance of 1/8 the recording aperture is suggested as a maximum reliable depth for a linearized tomographic inversion.

Nonlinear tomographic imaging (using multiple ray tracings with iterative model updates) improves the overall resolution of the output velocity model, especially increasing the depth to which a reliable image can be obtained. It also insures that the output velocity image is insensitive to the initial model. However, due to damping and smoothing in the tomography algorithm, the output image of a linear inversion is remarkably robust to a wide range of reasonable initial models. Oftentimes, a good initial model may be obtained manually from the picks or from regional information.

• *No offset grouping of picks versus required offset grouping of picks.* First-arrival tomography does not require that picks be manually grouped into offset branches common to a refracting interface, as does refraction statics. Rather, traveltimes from all offsets are simultaneously inverted to yield the complete velocity model. As a result, the number of parameters required for an accurate tomographic imaging is minimal. In addition, tomography appears to require less recording fold than refraction statics for a good solution.

As with refraction statics, first-arrival tomography is most sensitive to the accuracy of the time picks. First arrivals should be consistently picked, ensuring picked times are nearly identical for reciprocal raypaths (in split-spread recording). Poor tomography solutions are usually distinguished by abnormally high residuals (observed versus predicted traveltime differences), even after multiple iterations. Poor solutions may be caused by improper picks, limited recording aperture, insufficient or unevenly distributed ray coverage, geometry errors, etc.

Synthetic and real data examples suggest that first-arrival tomography may image near-surface velocities more accurately than refraction statics methods. Consequently, the shallow-velocity image estimated from tomography may provide for more accurate short and long wavelength statics. This is of significant benefit because it can result in an optimal NMO velocity analysis and CMP stack response (reflection events being more hyperbolic), better migration focusing and positioning, and a more reliable depth conversion. If needed, tomography velocities may be further utilized through the application of wave equation datuming or prestack depth migration. LE

Acknowledgments: The authors wish to thank J. Peters of UPRC for supporting this project. The idea presented began to form when X. Zhu was a doctoral candidate at the University of Texas-Dallas with Professor G. McMechan. We especially wish to acknowledge C. Stork and M. Brown at Advance Geophysical for providing finite-difference synthetic data, and J. Suydam, J. Breninger and R. McKinley for providing their field data. Helpful discussions from J. Suydam, J. Gibson, M. Schoomaker, D. Gish, S. Poe, T. Dean, R. Zinno, and G. Wilbourn are also appreciated. The data were processed by G. Kisselman, G. Wilbourn, and T. Lane. We also thank Union Pacific Resources for permission to publish.

Xianhuai Zhu is a senior geophysicist with Union Pacific Resources. He received his bachelor's in applied geophysics from the East China Petroleum Institute (now the China Petroleum University) in 1977 and a doctorate in geophysics from the University of Texas-Dallas in 1990. From 1977–85 he worked as a research geophysicist for the Research Institute of Geophysical Prospecting for Petroleum in China, and in 1985–86 he was a visiting scientist with the Cocorp project at Cornell University.

David Sixta received bachelor's and master's degrees from the Colorado School of Mines. He joined Golden Geophysical in 1981 and has been with Union Pacific Resources since 1985. He is currently manager of geophysical processing.

Burke Angstman is currently manager of exploration services for Union Pacific Resources. He previously worked for the US Geological Survey and Amoco Production Company. He received a bachelor's in applied mathematics from the University of the Pacific in 1975 and a master's in geophysics from Stanford University in 1978.